FORCE-MOMENT CAPABILITIES OF REVOLUTE-JOINTED PLANAR PARALLEL MANIPULATORS WITH ADDITIONAL ACTUATED BRANCHES

Flavio Firmani[1], Alp Zibil[1], Scott B. Nokleby[2], and Ron P. Podhorodeski[1†]

[1] Robotics and Mechanisms Laboratory, Department of Mechanical Engineering,
University of Victoria, P. O. Box 3055, Victoria, B. C, V8W 3P6, Canada.
{ffirmani, azibil, podhoro}@me.uvic.ca
[†]Corresponding author: Fax: (250)-721-6051

[2] Faculty of Engineering and Applied Science, University of Ontario Institute of Technology,
2000 Simcoe Street North, Oshawa, Ontario, L1H 7K4, Canada.
Scott.Nokleby@uoit.ca

Received June 2007, Accepted November 2007
No. 07-CSME-57, E.I.C. Accession 3026

ABSTRACT

The force-moment capabilities of revolute-jointed planar parallel manipulators (PPMs) are presented. A previously developed analysis that determines explicitly the force-moment capabilities of parallel manipulators is considered and the formulation is improved. This analysis is based upon properly adjusting the actuator outputs to their maximum capabilities. The force-moment capabilities of two actuation layouts are investigated: the non-redundant 3-RRR PPM and the redundantly actuated 4-RRR PPM, where the underline indicates the actuated joint. Four studies of force-moment capabilities are presented: maximum force with a prescribed moment, maximum applicable force, maximum moment with a prescribed force, and maximum applicable moment. These studies are performed for constant payload orientation of the mobile platform throughout the manipulator's workspace. It is concluded that the manipulator with the additional actuated branch shows an improvement of the force-moment capabilities at the expense of reducing its workspace.

CAPACITÉS DE FORCE ET MOMENT DES MANIPULATEURS PARALLÈLES PLANS AVEC ARTICULATIONS ROTOÏDES ET CHAÎNES ACTIONNÉES ADDITIONNELLES

RÉSUMÉ

Les capacités de force et moment des manipulateurs parallèles plans (MPPs) avec articulations rotoïdes sont présentées. Une analyse développée précédemment qui détermine explicitement les capacités de force et moment des manipulateurs parallèles est considérée et sa formulation est améliorée. Cette analyse est basée sur l'ajustement correct des couples des actionneurs au maximum de ses capacités. Les capacités de force et moment de deux dispositions d'actionnement sont étudiées: le MPP non redondant 3-RRR et le MMP avec actionnement redondant 4-RRR, où la lettre soulignée indique l'articulation actionnée. Quatre études des capacités de force et moment sont présentées: force maximale avec un moment prescrit, force maximale applicable, moment maximal avec une force prescrite, et moment maximal applicable. Ces études sont réalisées avec une orientation constante de la plate-forme mobile dans tout l'espace de travail du manipulateur. En conclusion, le manipulateur avec la chaîne actionnée additionnelle montre une amélioration des capacités de force et moment au prix d'une réduction de son espace de travail.

1 INTRODUCTION

1.1 Force Capabilities

This paper investigates the force-moment capabilities of planar parallel manipulators (PPMs) with revolute joints and how the inclusion of an additional actuated branch affects its performance. The mobile platform of PPMs is subject to the interaction of forces (f_y and f_x) along the plane and a moment (m_z) about the normal to the plane. For a specific moment m_z, the force capability of a PPM is defined as the maximum force that can be applied (or sustained) in any direction in the plane, $m_z = const.$ The force capability of a manipulator depends on its design, posture, and actuator capabilities. Consider the 3-RRR PPM described in the Appendix. Let the mobile platform be located at the centre of the workspace and the branches have the configuration shown in Figure 1a. The maximum output torque of the actuated joints is $\tau_{i_{\max}} = \pm 4.2$ Nm, for $i = 1, 2, 3$.

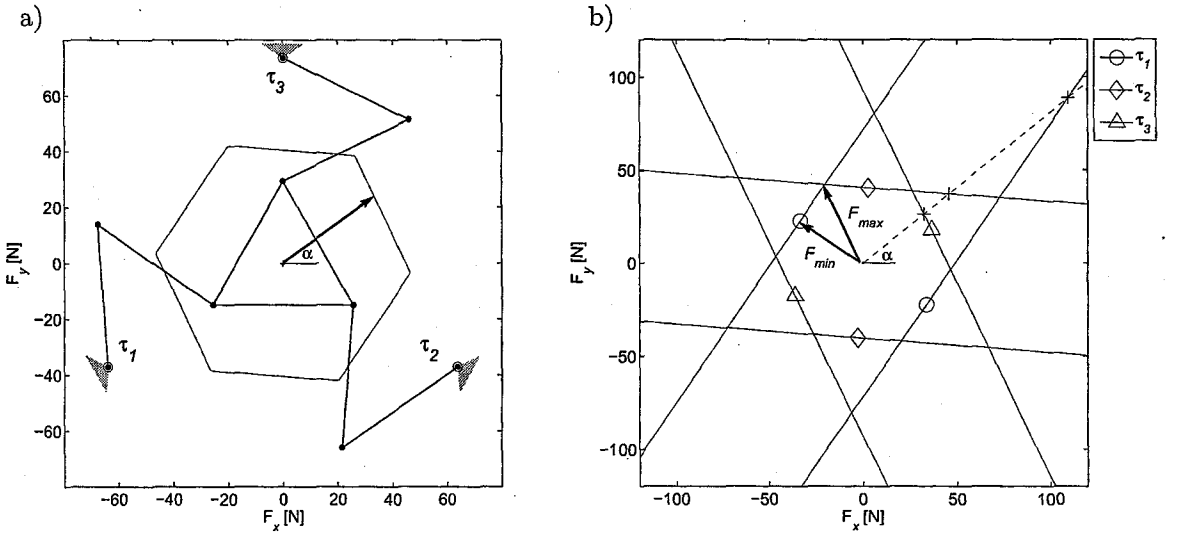

Figure 1: Generation of a Force Capability Polygon.

Force capabilities can be illustrated with force polygons. A force polygon shows the maximum forces that can be applied or sustained by the end-effector in any direction. Let α be any direction of the force, i.e., $0 \leqslant \alpha \leqslant 2\pi$. The hexagon shown in Figure 1a illustrates the force polygon of the described manipulator at $m_z = 0$. Force polygons may show elements of symmetry because the actuators provide the same torque output clockwise and counterclockwise, i.e., $\pm\tau_{i_{\max}}$. To generate a force polygon, consider the angle α shown in Figure 1b. The magnitude of the force in this direction (dashed line) is constrained by the actuator torque capabilities. Figure 1b illustrates the three points (denoted with +) in which the actuators are working at their maximum capabilities. The closest point to the centre of the force space constrains the force capability of the system because a greater force would imply that at least one actuator is working over its output capabilities. These points become lines when α is varied from 0 to 2π. Each actuator constrains the system with two parallel lines because of the positive and negative capabilities of the actuators ($\pm\tau_{i_{\max}}$). The area between these parallel lines represents the force that one actuator can sustain in any direction. The area enclosed by all the lines, a polygon, represents the force capabilities of the system. The distance from the centre of the force space to any point on the polygon is proportional to the magnitude of the force. Figure 1b also shows F_{max} and F_{min}, the maximum and the minimum of

the maximum applicable forces for all directions, respectively. These two magnitudes will be used to describe a force polygon.

The force-moment capability analysis is essential in the design and development of parallel manipulators. For a given application, the end-effector is subject to the interaction of forces and moments. Knowledge of the maximum forces and moments that the manipulator can apply or sustain is a necessary tool for an optimum design. By being able to graphically visualize the force-moment capabilities, comparisons between different design parameters, such as the actuator output and the dimensions of the links, can be explored.

The force-moment capability problem can be formulated as a constrained optimization problem. This problem involves an equality constraint denoted by the static force equation, $[\$'\mathbf{D}]\,\boldsymbol{\tau} = \mathbf{F}$, later derived in Section 2, and a set of inequality constraints representing the output range of the actuators. Hence,

$$\begin{aligned} &\text{maximize } f \quad \text{or} \quad \text{maximize } m_z \\ &\text{subject to: } [\$'\mathbf{D}]\,\boldsymbol{\tau} = \mathbf{F} \\ &\qquad -\tau_{i_{\max}} \leq \tau_i \leq \tau_{i_{\max}} \end{aligned} \tag{1}$$

where $[\$'\mathbf{D}]$ is a known numerical matrix defined by the geometry and the pose of the manipulator, $\mathbf{F} = \{f_x, f_y; m_z\}^{\mathrm{T}} = \{f\cos\alpha, f\sin\alpha; m_z\}^{\mathrm{T}}$ is the output wrench, with f and α being the magnitude and direction of the force, respectively; and $\tau_{i_{\max}}$ is the maximum output torque of the i^{th} branch.

Early works on force capabilities dealt with the problem of force distribution of two serial manipulators handling a common payload. Zheng and Luh [1] developed an algorithm that incorporates maximum torque output capabilities. Two analyses were presented. The first analysis ensured that the forces applied by the branches were in the same direction as the required force. The second analysis ensured that the load was evenly distributed between the two serial arms. Tao and Luh [2] considered minimizing the square of the joint torques of two joint-redundant cooperating manipulators. Kumar and Waldron [3] investigated force distribution in redundantly-actuated closed-loop kinematic chains and concluded that there would be zero internal force with the Moore-Penrose pseudo-inverse solution. Buttolo and Hannaford [4] analyzed the force capabilities of a redundant PPM. Torques were optimized using the ∞-norm resulting in higher force capabilities when compared to the pseudo-inverse solution. Nokleby *et al.* [5] developed a methodology to optimize the force capabilities of both non-redundantly and redundantly-actuated PPMs using a high norm and a scaling factor. All the previous papers involved optimization techniques that maximized either f or m_z. Zibil *et al.* [6] created an explicit methodology for determining the force-moment capabilities of redundantly actuated PPMs. Their methodology will be described and implemented in this work.

1.2 Redundancy

Merlet [7] described that the inclusion of redundancy may lead to improvements in various analyses such as forward kinematics, singular configurations, optimal force control, and calibration. Lee and Kim [8] defined a redundant parallel manipulator as one that has an infinite number of choices for either generating motion or resisting external forces. Also, Lee and Kim presented an analysis of different types of redundancy. Ebrahimi *et al.* [9] classified redundancy into two categories: kinematic and actuation redundancy.

Kinematic Redundancy

A manipulator is termed kinematically redundant when an infinite number of postures of the linkage lead to the same pose of the end-effector. Thus, there is an infinite number of possible solutions to the inverse kinematic problem. This is the typical case of redundant serial manipulators. For parallel manipulators, this redundancy happens when the number of joints of at least one branch is greater than the number of joints that are required to provide the desired mobility of the mobile platform. This type of redundancy allows self-motion of the redundantly-jointed branch(es) improving the dexterity and workspace of the manipulator. Also, kinematic redundancy can be implemented to reduce or even eliminate force-unconstrained (singular) configurations. Wang and Gosselin [10] added an extra revolute joint to one branch of the 3-RPR PPM yielding a RRPR-2RPR layout. The conditions that make this manipulator force unconstrained were identified and with actuation redundancy the singularity loci were reduced. Ebrahimi *et al.* [9] proposed a 3-PRRR layout, a manipulator which contains joint redundancy in every branch. By properly manipulating the two actuated joints of each branch, this manipulator can provide singularity free paths and obstacle avoidance. A draw back of this type of redundancy is the increase of mass and/or inertia due to the addition of actuators on mobile links. Despite the redundancy, there is only one vector force per branch acting on the mobile platform. Thus, the load capability cannot be optimized, but as an alternative, the direction of the branch forces can be optimized by changing the posture of the redundantly-jointed branch(es). With this type of redundancy, each actuator is manipulated independently and there are no internal forces that could damage the device.

Actuation Redundancy

A parallel manipulator is termed redundantly actuated when an infinite number of resultant force combinations can span the system of external forces. Thus, there is an infinite number of solutions to the forward static force problem. The implementation of this redundancy requires a reliable control system because a small variation in the displacement may cause severe damage to the manipulator. This redundancy may also be used to reduce force-unconstrained configurations. There are two types of actuation redundancy: in-branch redundancy and additional actuated branches.

In-Branch Redundancy. Passive joints are replaced by active joints. For every redundant actuator added within branch(es), the dimension of the forces resisting the external load is augmented by one. This type of redundancy can be easily incorporated into an existing device. Firmani and Podhorodeski [11] eliminated families of force-unconstrained configurations (singularities) by adding a redundant actuator to the 3-RRR PPM, yielding a RRR-2RRR layout. Nokleby *et al.* [5] and Zibil *et al.* [6] determined the force capabilities of the 3-RRR PPM by using an optimization-based method and an analytical-based method, respectively. Nokleby *et al.* [12] investigated the force-moment capabilities of different in-branch redundancy architectures. With in-branch redundancy, there is no change in the workspace of the manipulator. However, there is an increase of mass and/or inertia due to the addition of actuators on mobile links.

Additional Actuated Branches. An additional actuated branch is added to the system. For every additional actuated branch incorporated into the system, the number of forces acting on the mobile platform is augmented by one. This type of redundancy is of special interest when the first joint of each branch is being actuated, e.g., 4-PRR and 4-RRR PPMs, because there is no significant added mass onto the mobile links allowing the device to be considered for high speed applications. Buttolo and Hannaford [4] designed and analyzed the force capabilities of a 2-DOF 3-RRR PPM haptic device, where all three branches are pinned together. Firmani and Podhorodeski investigated the singularity loci of the 4-PRR PPM [13] and 4-RRR PPM [14]. The main problem of this design is the reduction of the dexterity and workspace of the manipulator.

In this work, a study of the force-capabilities of the 3-RRR and 4-RRR PPMs is carried out.

The design of these manipulators is presented in the Appendix.

The remainder of the paper is structured in the following form. The next section presents the derivation of the forward static force problem using screw theory. Then, the explicit methodology derived by Zibil *et al.* [6] is summarized and some aspects of its formulation are improved. Also, the force capabilities of the 3-RRR and 4-RRR PPMs are presented. The paper finishes with a discussion of the results and conclusions.

2 FORCE ANALYSIS

2.1 Screw Theory

A screw ($) is a line in space having an associated pitch. A screw quantity can be represented with the Plücker coordinates of a line summed with a term related to the screw direction multiplied by the pitch of the screw [15]. The angular velocity $\boldsymbol{\omega}$ and the translational velocity $\mathbf{v}$ of a point of a moving body may be represented by three-dimensional vectors that can be assembled into a screw quantity $\mathbf{V}$ called an instantaneous twist, $\mathbf{V} = \{\boldsymbol{\omega}^{\mathrm{T}}; \mathbf{v}^{\mathrm{T}}\}^{\mathrm{T}}$ [16]. The pitch of the twist is the ratio of the translational velocity to the angular velocity. The pitch of a twist is zero if there is pure rotational velocity about the screw axis, while the pitch of the twist is infinite if there is pure translational velocity along the screw axis.

On the other hand, the resultant force $\mathbf{f}$ and the moment $\mathbf{m}$ acting at a point on the body can be assembled into a similar screw quantity $\mathbf{F}$ called a wrench , $\mathbf{F} = \{\mathbf{f}^{\mathrm{T}}; \mathbf{m}^{\mathrm{T}}\}^{\mathrm{T}}$ [16]. The pitch of a wrench is the ratio of the moment to the force. A pure force is a wrench of zero pitch and a pure moment is a wrench of infinite pitch.

In general, the twist and the wrench are composed of six elements, i.e., for an instantaneous twist, there are three rotations about and three translations along a reference frame; while for a wrench there are three pure forces along and three moments about a reference frame. For a manipulator with $n-dof$, where $n < 6$, such as planar manipulators, the same $6-n$ coordinates of the joint twists and the output twist will be zero at any configuration [17]. For planar manipulators, the screw system of planar motion can be spanned by a rotation and two translations. Therefore, the instantaneous twist and the wrench will have only three non-zero coordinates. The twist is based on one angular velocity ω_z and two linear velocities v_x and v_y, i.e., $\mathbf{V} = \{\boldsymbol{\omega}^{\mathrm{T}}; \mathbf{v}^{\mathrm{T}}\}^{\mathrm{T}} = \{\omega_z; v_x, v_y\}^{\mathrm{T}}$. While the wrench is comprised of two forces f_x and f_y and one moment m_z, i.e., $\mathbf{F} = \{\mathbf{f}^{\mathrm{T}}; \mathbf{m}^{\mathrm{T}}\}^{\mathrm{T}} = \{f_x, f_y; m_z\}^{\mathrm{T}}$. Another way to express the wrench is $\mathbf{F} = \{f\cos\alpha, f\sin\alpha; m_z\}^{\mathrm{T}}$, where f and α are the magnitude and direction of the force, respectively.

The forces that can be applied (sustained) by a branch can be modelled with associated reciprocal screws [15]. The force exerted by the k^{th} actuated joint of the i^{th} branch is characterized by an associated reciprocal screw, $\$'_{k_i}$, reciprocal to all joints of the i^{th} branch except for the actuated joint k, i.e.,

$$\$_{j_i} \circledast \$'_{k_i} = 0, \text{ for } j \neq k \tag{2}$$

where $\$_{j_i}$ denotes the screw coordinates of all joints $j \neq k$ of the i^{th} branch and $\circledast$ denotes the reciprocal product between two screws. If $\mathbf{V} = \{\omega_z; v_x, v_y\}^{\mathrm{T}}$ and $\mathbf{F} = \{f_x, f_y; m_z\}^{\mathrm{T}}$ then $\mathbf{V} \circledast \mathbf{F} = \omega_z m_z + v_x f_x + v_y f_y$.

2.2 Forward Static Force Solution

The wrench applied by a parallel manipulator is the sum of wrenches applied by all m actuated joints of the manipulator. In matrix form, the static force solution results:

$$\mathbf{F}_{3\times1} = [\$']_{3\times m}\,\mathbf{w}_{m\times1} \tag{3}$$

where $[\$']$ is referred to as the associated reciprocal screw matrix and $\mathbf{w}$ the vector of wrench intensities.

The torque applied by the k^{th} actuated joint of the i^{th} branch can be modelled as:

$$\tau_{k_i} = w_{k_i}\left(\$_{k_i} \circledast \$'_{k_i}\right) \tag{4}$$

Therefore, the wrench intensity is

$$w_{k_i} = \frac{\tau_{k_i}}{\left(\$_{k_i} \circledast \$'_{k_i}\right)} \tag{5}$$

The relationship among all the wrench intensities in the system yields:

$$\mathbf{w} = [\mathbf{D}]\,\boldsymbol{\tau} \tag{6}$$

where $[\mathbf{D}]$ is a diagonal matrix whose entries are $1/(\$_{k_i} \circledast \$'_{k_i})$.

Combining Eqs. (3 and 6) results in the forward static force solution, i.e.,

$$[\$'\mathbf{D}]_{3\times m}\,\boldsymbol{\tau}_{m\times1} = \mathbf{F}_{3\times1} \tag{7}$$

where $[\$'\mathbf{D}] = [\$']\,[\mathbf{D}]$. This matrix is also referred in the literature to as $[\mathbf{J}]^{-\mathrm{T}}$, with $[\mathbf{J}]$ being the Jacobian of the manipulator.

3 Force-Moment Capabilities

3.1 Maximum Output Capabilities

Nokleby *et al.* [5] noticed that greater output wrenches are obtained when the individual actuators are close to their maximum capabilities. Zibil *et al.* [6] developed a solution which explicitly sets the largest number of actuators to their maximum output capabilities. The actuators are set to their maximum capabilities by rearranging Eq. (7) as a linear system of equations of the form $\mathbf{Ax} = \mathbf{b}$. The reader is referred to [6] for more details on the assembling of this linear system of equations. Both works [5] and [6] considered the direction α to be varied from 0 to 2π by assuming small increments. This approach can be computationally expensive and also can be inaccurate because the maximum forces will most likely occur within intervals of α. In this paper, the direction is considered as an unknown variable. As a result, a much more accurate solution of the maximum (F_{max}) and the minimum (F_{min}) of the maximum applicable (sustainable) forces of the force polygon can be determined.

In the following sub-sections four studies of force-moment capabilities of the 3-RRR and 4-RRR PPMs with constant payload orientation will be presented: maximum force with a prescribed moment, maximum applicable force, maximum moment with a prescribed force, and maximum applicable moment. The characteristics of these manipulators are described in the Appendix. The results of these studies are presented in Figures 2 and 3. Note that some force-moment capability results have been excluded from the plots because their values were very large compared to the rest of the results in the workspace due to their close proximity to a singular configuration ; consequently, a better overall greyscale gradient results.

3.2 Maximum Force with a Prescribed Moment

Let m_z be a prescribed quantity. The vertices of the force polygon of the 3-RRR PPM are found by setting two actuators to their maximum output capabilities ($\tau_{m\,1}$ and $\tau_{m\,2}$). This is shown in Figure 1b, where vertices are formed with the intersection of two lines. The third actuator will be working within its output range and will be referred to as being in transition (τ_t). Mathematically, Eq. (7) contains five unknown variables, i.e., f_x, f_y, and τ_i for $i = 1, 2, 3$. By assuming two actuator torques to be evaluated at their maximum output capabilities, a fully constrained system results. Thus, Eq. (7) may be rearranged as $\mathbf{Ax} = \mathbf{b}$, where $\mathbf{x} = \begin{bmatrix} f_x & f_y & \tau_t \end{bmatrix}^{\mathrm{T}}$, i.e.,

$$[\$'\mathbf{D}]_{3\times m}\,\boldsymbol{\tau}_{m\times 1} = \mathbf{F}_{3\times 1} \Rightarrow \mathbf{Ax} = \mathbf{b} \tag{8}$$

$$\begin{bmatrix} \$'D_{1,1} & \$'D_{1,2} & \$'D_{1,3} \\ \$'D_{2,1} & \$'D_{2,2} & \$'D_{2,3} \\ \$'D_{3,1} & \$'D_{3,2} & \$'D_{3,3} \end{bmatrix} \begin{bmatrix} \tau_1 \\ \tau_2 \\ \tau_3 \end{bmatrix} = \begin{bmatrix} f_x \\ f_y \\ m_z \end{bmatrix} \Rightarrow \tag{9}$$

$$\underbrace{\begin{bmatrix} 1 & 0 & -\$'D_{1,t} \\ 0 & 1 & -\$'D_{2,t} \\ 0 & 0 & -\$'D_{3,t} \end{bmatrix}}_{\mathbf{A}} \underbrace{\begin{bmatrix} f_x \\ f_y \\ \tau_t \end{bmatrix}}_{\mathbf{x}} = \underbrace{\begin{bmatrix} \$'D_{1,m\,1} & \$'D_{1,m\,2} \\ \$'D_{2,m\,1} & \$'D_{2,m\,2} \\ \$'D_{3,m\,1} & \$'D_{3,m\,2} \end{bmatrix} \begin{bmatrix} \pm\tau_{m\,1} \\ \pm\tau_{m\,2} \end{bmatrix} - \begin{bmatrix} 0 \\ 0 \\ m_z \end{bmatrix}}_{\mathbf{b}} \tag{10}$$

All possible combinations of torques at their maximum and torque signs are considered. There are 12 combinations in total, i.e., three torques at the maximum combinations (two out of three output torques) and four sign combinations (each one of the two maximized torques can be either positive or negative). All combinations are evaluated and the force polygon is generated by enclosing the solutions where the torque in transition does not exceed its torque output capabilities. The maximum of the maximum forces, F_{max}, corresponds to the largest value of f that can be evaluated with the combinations. The minimum of the maximum forces, F_{min}, is determined by finding the shortest distance between the polygon and the centre of the force space. Assume a pure force problem, i.e., $m_z = 0$. Figures 2a and 2b illustrate the pure force capabilities of the 3-RRR PPM, F_{min} and F_{max}, respectively.

For the 4-RRR PPM, three actuators can be set to their maximum capabilities. There are 32 combinations, i.e., four torques at their maximum combinations (three out of four actuators) and eight sign combinations (each one of the three maximized torques can be $\pm\tau_{i_{\max}}$). The general equation that provides the number of combinations for any m actuated branches is $n_c = 2^{m-1}m$. Figures 3a and 3b show the pure force capabilities (F_{min} and F_{max}, respectively) throughout its workspace.

3.3 Maximum Applicable Force

The maximum force that can be applied by the manipulator has an associated moment. This moment m_z can be considered as an unknown value. Since there are $3+m$ unknown variables, i.e., f_x, f_y, m_z, and τ_i for $i = 1, \ldots, m$, in Eq. (7), all actuator outputs can be set to their maximum capabilities. This yields a linear system of the form $\mathbf{Ax} = \mathbf{b}$, where $\mathbf{x} = \begin{bmatrix} f_x & f_y & m_z \end{bmatrix}^{\mathrm{T}}$. The number of combinations is based on the number of actuated branches and is given by the following equation: $n_c = 2^m$. That is, there are 8 and 16 combinations for the 3-RRR and 4-RRR PPMs, respectively. For each pose of the manipulator, these points may be plotted in a force-moment space, i.e., $f_x - f_y - m_z$. The volume contained within these points represent the region in which the manipulator is capable of applying or sustaining an output wrench. By projecting these points on the force plane, a force polygon is generated.

For the 3-RRR PPM, Figures 2c and 2d show the minimum (F_{min}) and maximum (F_{max}) force capabilities, respectively; while, Figures 2e and 2f illustrate their associated moments. Similarly, the corresponding plots in Figure 3 show the maximum forces and associated moments of the 4-RRR PPM.

3.4 Maximum Moment with a Prescribed Force

The maximum moment that can be applied with a prescribed force leads to a system of $1 + m$ unknown variables, i.e., m_z, and τ_i for $i = 1, \ldots, m$, while f_x and f_y are known quantities. Hence,

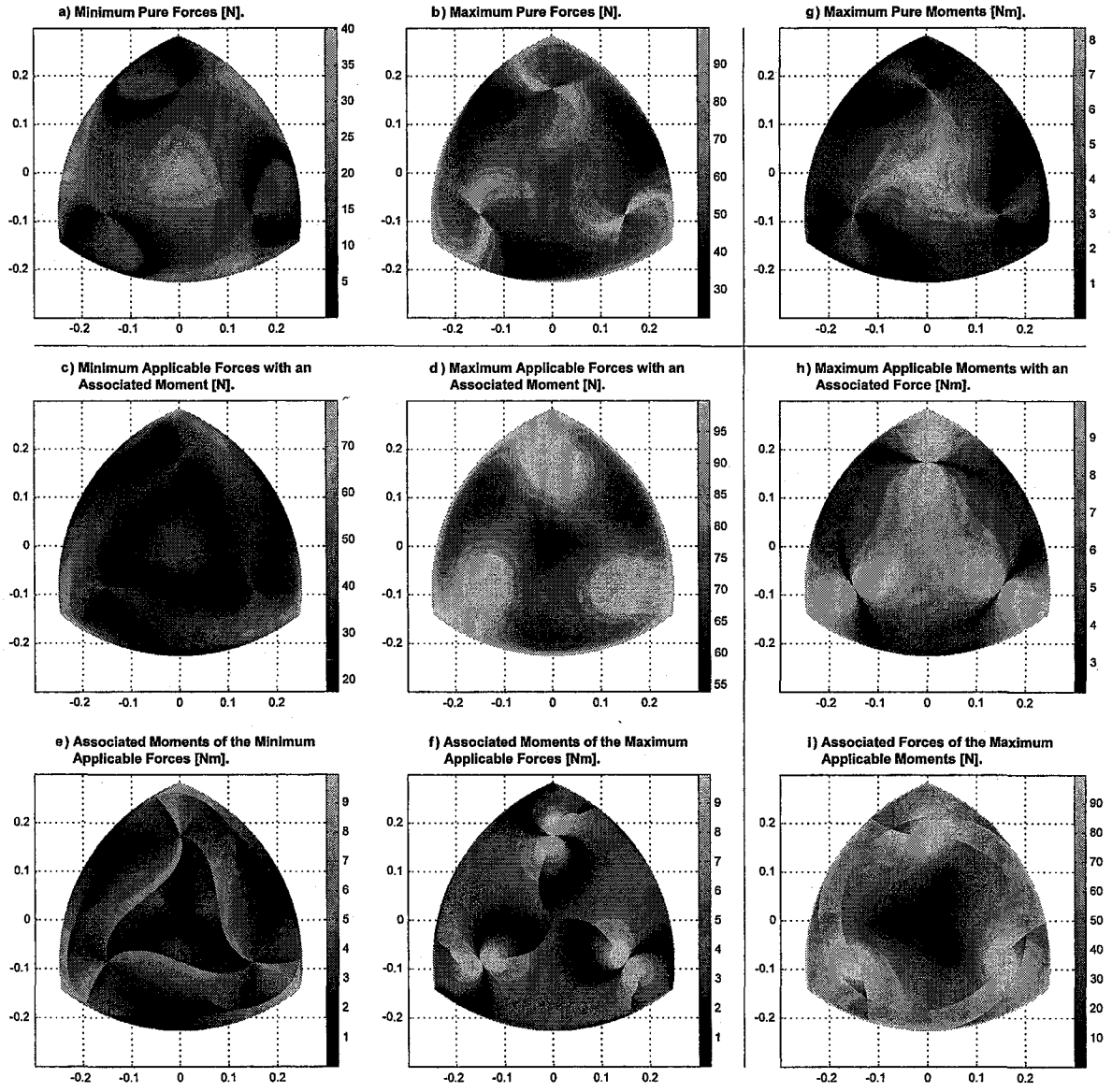

Figure 2: Force-Moment Capabilities of the 3-RRR PPM Throughout its Workspace. The X and Y Axes Define the Workspace [m] and the Greyscale Represents either Forces [N] or Moments [Nm].

two actuator outputs will be in transition (τ_{t_a} and τ_{t_b}). This yields a linear system of the form $\mathbf{Ax} = \mathbf{b}$, where $\mathbf{x} = \begin{bmatrix} m_z & \tau_{t_a} & \tau_{t_b} \end{bmatrix}^T$. The number of possible combinations is based on the number of actuated branches and is given by the following equation: $n_c = 2^{m-3}(m-1)m$. That is, there are 6 and 24 combinations for the 3-RRR and 4-RRR PPMs, respectively. Combinations are evaluated and the resulting largest m_z, where the torques in transition do not exceed their torque output capabilities, yields the maximum moment with a prescribed force.

Figures 2g and 3g show the pure moment capabilities ($f = 0$) of the 3-RRR and 4-RRR PPMs, respectively.

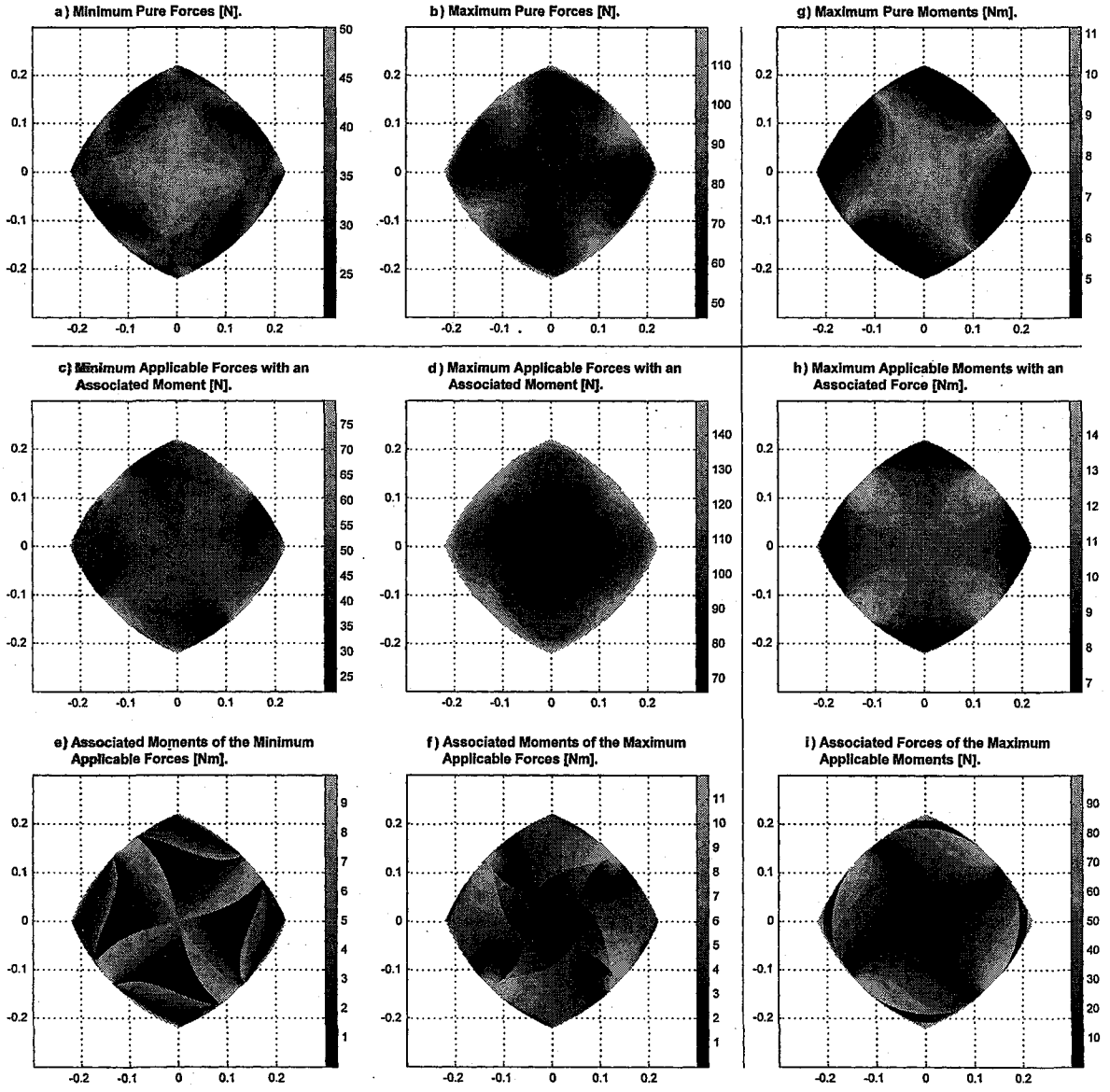

Figure 3: Force-Moment Capabilities of the 4-RRR PPM Throughout its Workspace. The X and Y Axes Define the Workspace [m] and the Greyscale Represents either Forces [N] or Moments [Nm].

3.5 Maximum Applicable Moment

The maximum moment that can be applied by the manipulator has an associated force. There are $3+m$ unknown variables, i.e., f_x, f_y, m_z, and τ_i for $i = 1, \ldots, m$. Since only m_z has to be maximized, one equation based on the signs of the last row of matrix $[\$'\mathbf{D}]_{3\times m}$ in Eq. (7) has to be evaluated: $(\$'D_{3,1})(\tau_{1_{\max}}) + (\$'D_{3,2})(\tau_{2_{\max}}) + \ldots + (\$'D_{3,m})(\tau_{m_{\max}}) = m_z$. Two solutions exist for m_z, the maximum positive moment is obtained by making all the monomials positive; while, the maximum negative moment occurs when all the monomials are negative.

Figures 2h and 3h show the maximum applicable moment of the 3-RRR and 4-RRR PPMs, respectively. Figures 2i and 3i illustrate their associated forces.

4 Discussion

The inclusion of an additional branch enhances the force-moment capabilities of the manipulator. At first glance, the greyscale range of every plot shows a clear improvement for the manipulator with redundancy. Each plot was generated with approximately 2×10^5 loci of locations. The number of excluded values in the capped figures was kept even between the two manipulators. Also, note that the workspaces of the 4-RRR PPM in Figure 3 are reduced in comparison to the workspaces of the 3-RRR PPM in Figure 2.

A more detailed analysis is presented with some numerical indices. This comparison should be carefully taken in hand because some of kinematic properties, such as singularities and reachable workspace, of the 3-RRR and 4-RRR PPMs are different.

Nokleby *et al.* [12] described how force-moment capabilities tend to increase towards infinity around locations in which the manipulator is at or near a singular configuration. For each manipulator, these singularities occur at different locations. A comparison of the results presented in Figures 2 and 3 is carried out with indices that are not affected by large values. Maximum values are not considered because they generally occur near singular configurations.

Table 1: Median and Minimum Values of the Force [N] and Moment [Nm] Capability Studies.

Study I: Maximum Force with a Prescribed Moment (Pure force $m_z = 0$)

	$\tilde{F}_{\min}$	$\min(F_{\min})$	$\tilde{F}_{\max}$	$\min(F_{\max})$	
3-RRR PPM	17.13	0	57.11	22.33	Figures 2a and 2b
4-RRR PPM	34.47	20.61	66.24	46.3	Figures 3a and 3b

Study II: Maximum Applicable Force with Associated Moments

	$\tilde{F}_{\min}$	$\min(F_{\min})$	$\tilde{F}_{\max}$	$\min(F_{\max})$	
3-RRR PPM	31.22	17.41	79.76	53.8	Figures 2c and 2d
4-RRR PPM	46.14	22.02	92.14	66.06	Figures 3c and 3d

Study III: Maximum Moment with a Prescribed Force (Pure moment $f = 0$)

	$\tilde{m}_z$	$\min(m_z)$	
3-RRR PPM	2	0	Figure 2g
4-RRR PPM	7.01	4.06	Figure 3g

Study IV: Maximum Applicable Moment with Associated Forces

	$\tilde{m}_z$	$\min(m_z)$	
3-RRR PPM	6.87	2.21	Figures 2h
4-RRR PPM	11.06	6.75	Figures 3h

The most significant plots that were not capped are the minimum pure forces (Figures 2a and 3a) and the pure moments (Figures 2g and 3g). For 3-RRR PPM, $\max(F_{\min}) = 40.35$ N and $\max(m_z) = 8.4$ Nm; while, for the 4-RRR PPM, $\max(F_{\min}) = 50.39$ N and $\max(m_z) = 11.2$ Nm.

In this work, minimum and median values are adopted as indices of comparison. Minimum values show the global minimum of either $F_{\min}$ or $F_{\max}$ that can be sustained at any location in the workspace. The median is preferred over the mean because the results of the mean are affected by large values. The median is an adequate index due to the large amount of data values considered and the nature of the plots, which represent smooth surfaces.

The median ($\tilde{*}$) and minimum values ($\min(*)$) of all the force-moment capability studies are summarized in Table 1. The force-moment capabilities of the 4-RRR PPM show a marked improvement over the results obtained with the 3-RRR PPM. Indices of the associated moments or forces (last row of plots) were omitted because the objective of Studies II and IV was to maximize forces and moments, respectively. The associated values are merely resultants of their corresponding studies.

5 Conclusion

A previously developed methodology for determining the force-moment capabilities of parallel manipulators was improved by considering the direction of the force as an unknown variable. Herein, the direction of the force is determined analytically. The proposed methodology turned out to be more accurate and more computationally efficient. The force-moment capability analysis was formulated with concepts of screw quantities and kinematic analysis. It was implemented for the non-redundant 3-RRR PPM and the redundant 4-RRR PPM layouts. Four different studies of force-moment capabilities were presented and it was shown that in every study the inclusion of an additional branch improved the force-moment capabilities of the manipulator at the expense of its dexterity and reachability.

References

[1] Y. F. Zheng and J. Y. S. Luh, "Optimal Load Distribution for Two Industrial Robots Handling a Single Object," in *Proceedings of the 1988 IEEE International Conference on Robotics and Automation*, (Philadelphia, PA, USA), pp. 344–349, April 24-29, 1988.

[2] J. M. Tao and J. Y. S. Luh, "Coordination of Two Redundant Manipulators," in *Proceedings of the 1989 IEEE International Conference on Robotics and Automation*, (Scottsdale, AZ, USA), pp. 425–430, May 14-19, 1989.

[3] V. Kumar and K. J. Waldron, "Force Distribution in Closed Kinematic Chains," in *Proceedings of the 1988 IEEE International Conference on Robotics and Automation*, (Philadelphia, PA, USA), pp. 114–119, April 24-29, 1988.

[4] P. Buttolo and B. Hannaford, "Advantages of Actuation Redundancy for the Design of Haptic Displays," in *Proceedings of the 1995 ASME International Mechanical Engineering Congress and Exposition–Part 2*, (San Francisco, CA, USA), pp. 623–630, November 12-17, 1995.

[5] S. B. Nokleby, R. Fisher, R. P. Podhorodeski, and F. Firmani, "Force Capabilities of Redundantly-Actuated Parallel Manipulators," *Mechanism and Machine Theory*, vol. 40, no. 5, pp. 578–599, 2005.

[6] A. Zibil, F. Firmani, S. B. Nokleby, and R. P. Podhorodeski, "An Explicit Method for Determining the Force-Moment Capabilities of Redundantly-Actuated Planar Parallel Manipulators," *Transactions of the ASME, Journal of Mechanical Design*, vol. 129, no. 10, pp. 1046–1055, 2007.

[7] J. P. Merlet, "Redundant Parallel Manipulators," *Journal of Laboratory Robotics and Automation*, vol. 8, pp. 17–24, 1996.

[8] S. Lee and S. Kim, "Kinematic Analysis of Generalized Parallel Manipulator Systems," in *Proceedings of the 32nd IEEE Conference on Decision and Control*, vol. 2, (San Antonio, TX, USA), pp. 1097–1102, December 15-17, 1993.

[9] I. Ebrahimi, J. A. Carretero, and R. Boudreau, "3-PRRR Redundant Planar Parallel Manipulator: Inverse Displacement, Workspace and Singularity Analyses," *Mechanism and Machine Theory*, vol. 42, no. 8, pp. 1007–1016, 2007.

[10] J. Wang and C. M. Gosselin, "Kinematic Analysis and Design of Kinematically Redundant Parallel Mechanisms," *Transactions of the ASME, Journal of Mechanical Design*, vol. 126, no. 1, pp. 109–118, 2004.

[11] F. Firmani and R. P. Podhorodeski, "Force-Unconstrained Poses for a Redundantly-Actuated Planar Parallel Manipulator," *Mechanism and Machine Theory*, vol. 39, no. 5, pp. 459–476, 2004.

[12] S. B. Nokleby, F. Firmani, A. Zibil, and R. P. Podhorodeski, "Force-Moment Capabilities of Redundantly-Actuated Planar-Parallel Architectures," Proceedings of the IFToMM 2007 World Congress, (Besançon, France), 6 pages, June 17-21, 2007.

[13] F. Firmani and R. P. Podhorodeski, "Force-Unconstrained Poses of the 3-PRR and 4-PRR Planar Parallel Manipulators," *Transactions of the CSME*, vol. 29, no. 4, pp. 617–628, 2005.

[14] F. Firmani and R. P. Podhorodeski, "Singularity Loci of Revolute-Jointed Planar Parallel Manipulators with Redundant Actuated Branches," Proceedings of the IFToMM 2007 World Congress, (Besançon, France), 6 pages, June 17-21, 2007.

[15] K. H. Hunt, *Kinematic Geometry of Mechanisms*. Toronto, ON, Canada: Oxford University Press, 1978.

[16] R. S. Ball, *A Treatise of the Theory of Screws*. New York, NY, USA: Cambridge University Press, 1900.

[17] D. Zlatanov, R. G. Fenton, and B. Benhabib, "Analysis of the instantaneous kinematics and singular configurations of hybrid-chain manipulators," in *Proceedings of the ASME 23rd Biennial Mechanisms Conference*, vol. 72, (Minneapolis, MN, USA), pp. 467–476, 1994.

[18] R. Fisher, R. P. Podhorodeski, and S. B. Nokleby, "A Reconfigurable Planar Parallel Manipulator," *Journal of Robotic Systems*, vol. 21, no. 12, pp. 665–675, 2004.

APPENDIX

The two revolute-jointed planar parallel manipulators used in this paper are shown in Figure 4. The dimensions and the actuator capabilities of the 3-RRR PPM are modeled after the Reconfigurable Planar Parallel Manipulator (RPPM) designed by Fisher *et al.* [18]. This manipulator is comprised of two equilateral triangle platforms (base and mobile) that are connected by three branches, as shown in Figure 4a. The design of the 4-RRR PPM involves two square platforms connected by four branches, as illustrated in Figure 4b. Each branch of these manipulators contains two links and three revolute joints. The first joints are active (actuated), while the second and third joints are passive joints. In Figure 4, the active joints are indicated with circles. The dimensions of both platforms are similar. The base and mobile platform edge lengths are 0.5 m and 0.2 m, respectively. The lengths of the first and second links of each branch are 0.2 m. The maximum output torque capabilities of the actuators (based on the existing actuators of the RPPM) is ± 4.2 Nm.

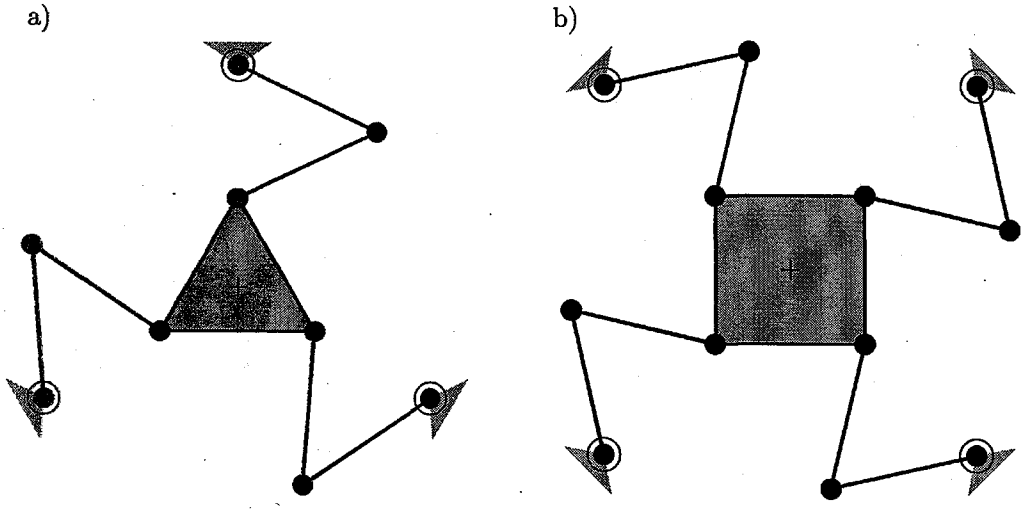

Figure 4: Planar Parallel Manipulators with Revolute Joints.